magnetism

MDPI

Article

Characterization of Electromagnetic Field Interaction with a Cylinder Situated Between Two Half-Spaces

Mohamed Elkattan

Department of Electronics, Nuclear Materials Authority, Cairo 11728, Egypt; emtiazegf@hotmail.com

Abstract

The development of efficient and accurate methods for analyzing electromagnetic scattering by cylindrical objects has theoretical and practical relevance due to its importance in photonics, optoelectronics, antennas, and remote sensing applications. Modal methods are a category of semi-analytical solvers used in modelling electromagnetic scattering problems. Modal methods have several advantages compared to fully numerical methods, and they are very useful for problems with translational symmetry. In this paper, the interaction of electromagnetic waves with a cylinder with an impedance surface situated between two homogeneous half-spaces with different electromagnetic properties is studied. A forward model of the addressed scattering problem is presented. A theoretical formulation of the problem is deduced within a flexible and comprehensive framework that can be extended to solve other related cylindrical configurations. Furthermore, the modal solver developed within the proposed framework can be further developed to consider other forms of source excitations. Moreover, the impedance-dominant scenario has been investigated, and a convergent scheme has been derived for the special case within this regime.

Keywords: electromagnetism; scattering; impedance boundary condition; impedance-dominant regime

1. Introduction

The characterization of electromagnetic field interaction with many scatterers is an extremely significant topic driven by rapidly evolving technological applications [1–3]. Several electromagnetic and photonic applications require the modelling of electromagnetic wave scattering with diverse structures embedded within different geometries [4–8]. The development of efficient solvers to represent the forward model can be a challenging task depending on the examined configuration [9–12]. Characterizing scattering phenomena in media comprising cylindrical structures may be done by means of conventional techniques that mostly rely on dealing with Maxwell's differential equations numerically, such as finite element and finite difference approaches [13,14]. However, many challenges arise in handling such structures through applying these numerical approaches, such as imposing unphysical non-reflecting boundaries and difficulties in the representation of highly localized sources, in addition to numerical dispersion and numerical polarization [15–17]. Therefore, it is of interest to develop new approaches that avoid these drawbacks and efficiently model the intended configuration.

An interesting category of approaches that avoid discretizing the entire problem domain is that of modal methods. Generally, modal methods are approaches that use semi-analytical techniques, where the fields are expanded in terms of a set of eigenfunctions

Academic Editor: Massimo Donelli

Received: 6 March 2026
Revised: 25 April 2026
Accepted: 29 April 2026
Published: 5 May 2026

that satisfy Maxwell's equations and boundary conditions in a given geometry [18,19]. Different modal approaches have been applied to cylindrical configurations similar to the one studied in this paper. In [20,21], approaches were developed to treat the plane wave scattering by a conducting cylinder partially buried in a ground plane for both TM and TE polarization cases. The scattering by a metallic cylinder on a substrate, with consideration of the burying effect, was discussed in [22]. Another approach was developed in [23] to address the scattering by buried dielectric cylindrical structures. The plane wave scattering by a finite set of perfectly conducting or dielectric cylinders buried in a dielectric half-space was considered in [24]. The scattering by a metallic cylinder buried in a lossy medium was studied in [25]. Another study [26] investigated the scattering of a perfect electromagnetic conducting (PEMC) circular cylinder buried inside a half-space.

In these modal approaches, fields are expanded using Fourier series in the angular variable. Thus, the resultant solutions in these approaches present intrinsically coupled modal structures that require the solution of dense matrix systems and may exhibit algebraic convergence behaviour [27]. In this paper, modelling of the interaction of electromagnetic fields with a cylindrical object situated between piecewise homogeneous media comprising two homogeneous half-spaces with asymmetric electromagnetic properties is investigated. A proposed novel approach is introduced in this work to solve this scattering problem, where the theoretical model formulations are derived with the proper boundary conditions to delineate the electromagnetic fields of the studied configuration. Unlike other modal approaches, the solution in this paper incorporates an exponential convergence feature and diagonal matrix systems. Furthermore, the deduced fields' representations offer a flexible framework that enhances the ability to model electromagnetic scattering in versatile scenarios involving similar configurations. From the same perspective, the impedance-dominant regime is addressed in this paper, and proposed treatments are developed in this work to analyze electromagnetic fields in a special case within this regime.

2. Forward Solver Procedure

The proposed forward solver in this work is formulated to model electromagnetic fields in the presence of an impedance cylindrical scatterer situated between two different media, upper and lower media, which may have dissimilar electromagnetic properties. The permittivity and permeability of the upper medium are denoted as ϵ_u and μ_u respectively, while the permittivity and permeability of the lower medium are denoted as ϵ_l and μ_l respectively. The model investigated in this paper is illustrated in Figure 1. The interface between the two media is the Y = 0 plane, while the axis of the cylinder is the z-axis of the Cartesian coordinate system. The cylinder has a surface impedance, Z_c, and a radius, r. The scatterer is illuminated by a time-harmonic electric line current source in the z-direction located at the $(\rho',\ \varphi')$ cylindrical coordinates. Furthermore, a harmonic time dependence of the form $e^{-i\omega t}$ is assumed, and it will be suppressed accordingly in further analyses. For this problem, due to the symmetrical nature of the examined structure relative to the $\varphi = \pm\frac{\pi}{2}$ plane, the boundary conditions in the symmetry plane are equivalent to either a perfect magnetic conductor (PMC) or a perfect electric conductor (PEC). Thus, without loss of generality, the analysis derived in this paper will apply to the PMC wall case only. That is, the presented approach deals with the transverse electric (TE) polarization case.

https://doi.org/10.3390/magnetism6020017

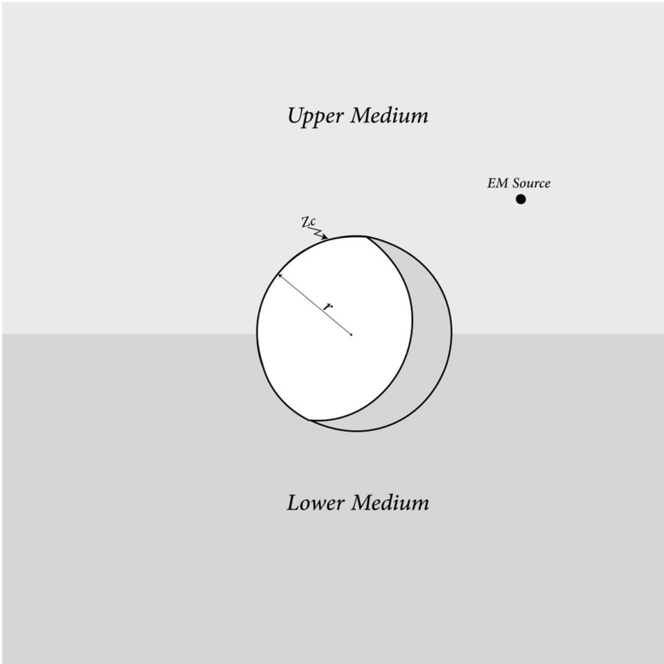

Figure 1. The model investigated in this work.

The solution scheme offered for the targeted problem begins with representing the z-directed magnetic field components by means of a series formulation of the incident and scattered fields. Here, the magnetic field of the upper medium in the z-direction, H_z^u, can be defined as the sum of a field, $H_z^{u(d)}$, which represents the source discontinuity in the φ-direction, and an additional field, $H_z^{u(a)}$, which represents the rest of the field of the upper medium. $H_z^{u(d)}$ and $H_z^{u(a)}$ can be written as

$$H_z^{u(d)} = \sum_i \left[\frac{\sin\{\nu_{ui}(\pi/2 - \varphi_>)\}\cos\{\nu_{ui}\varphi_<\}}{2\nu_{ui}\cos\nu_{ui}\frac{\pi}{2}} \Psi_i(k_u\rho') \right] \Psi_i(k_u\rho), \tag{1}$$

$$H_z^{u(a)} = \sum_i S_u(\nu_{ui})\sin\left\{\nu_{ui}\left(\varphi - \frac{\pi}{2}\right)\right\}\Psi_i(k_u\rho). \tag{2}$$

Accordingly, the magnetic field of the lower medium in the z-direction, H_z^l, can be written as

$$H_z^l = \sum_i S_l(\nu_{li})\sin\left\{\nu_{li}\left(\varphi + \frac{\pi}{2}\right)\right\}\Psi_i(k_l\rho), \tag{3}$$

where i is the number of indices, $S_{u.l}$ are the expansion coefficient vectors of the upper and lower media respectively, and $k_u = w\sqrt{\mu_u\epsilon_u}$ and $k_l = w\sqrt{\mu_l\epsilon_l}$ are the upper and lower medium wavenumbers respectively. Notably, once the H_z field components are computed, the rest of the field components of the problem can be derived as

$$E_\rho = \frac{j}{\omega\epsilon}\frac{1}{\rho}\frac{\partial H_z}{\partial\varphi}, \text{ and} \tag{4}$$

$$E_\varphi = \frac{-j}{\omega\epsilon}\frac{\partial H_z}{\partial\rho}. \tag{5}$$

So, by utilizing the proposed wave interaction scheme within the investigated model, the fields are formulated as a series representation over unidentified expansion coefficients for an index transform, where the transform pair is given by

$$f(\rho) = \sum_i S_i\Psi_i(k\rho), \tag{6}$$

$$S_i = \int_r^{\infty} \frac{1}{\rho} f(\rho)\, \Psi_i(k\rho)\, d\rho/\rho\,. \tag{7}$$

$\Psi_i(k\rho)$ is a complete orthonormal set that is defined as

$$\Psi_i(k\rho) = N_c\, H_{v_i}^{(1)}(k\rho), \tag{8}$$

where $H_{v_i}^{(1)}(k\rho)$ is the Hankel function of type one with a v_i index and $k\rho$ argument and $\{v_i\}$ is the set of complex roots located at $d(v_i) = 0$ in the first quadrant of the complex v plane. N_c is the normalization constant, which is defined as

$$N_c = \left\{ -j\pi \frac{v_i\, b(v_i)}{\left[\frac{\partial d(\nu)}{\partial v}\right]_{\nu_i}} \right\}^{0.5} H_{\nu_i}^{(1)}(k\rho), \tag{9}$$

$$\text{where } b(\nu) = J_v'(kr) + j\overline{D}\, J_v(kr), \tag{10}$$

$$d(\nu) = H_v'^{(1)}(kr) + j\overline{D}\, H_\nu^{(1)}(kr), \tag{11}$$

$$\text{and } J_v'(z) = \frac{dJ_\nu(z)}{dz}, \tag{12}$$

$$H_v'^{(1)}(z) = \frac{dH_\nu^1(z)}{dz}, \tag{13}$$

$J_\nu(z)$ is the Bessel function and $H_\nu^1(z)$ is the Hankel function of type one. $\overline{D} = {Z_{l,u}}/{Z_c}$, where $Z_{l,u} = \sqrt{{\mu_{l,u}}/{\epsilon_{l,u}}}$, is the impedance of medium 1 and medium 2 respectively. Notably, the passivity requirement is met if the real part of $(\overline{D}) \geq 0$. At the interface between the upper and lower media, the boundary conditions imply that

$$H_z^{u(d)} + H_z^{u(a)} = H_z^l \quad at\ \varphi = 0, \tag{14}$$

$$\frac{1}{\epsilon_u}\left(\frac{\partial H_z^{u(d)}}{\partial \varphi} + \frac{\partial H_z^{u(a)}}{\partial \varphi} \right) = \frac{1}{\epsilon_l} \frac{\partial H_z^l}{\partial \varphi} \qquad at\ \varphi = 0. \tag{15}$$

Furthermore, the continuity of the tangential field components applies at the interface between the upper and lower media, which implies that

$$\begin{gathered} \sum\nolimits_i \left\{ \frac{\sin \nu_{ui}\, \left(\frac{\pi}{2} - \varphi'\right)}{2v_{ui}\, \cos \nu_{ui}\, \frac{\pi}{2}}\, \Psi_i(k_u\rho') - S_u(\nu_{ui})\, \sin\!\left(\nu_{ui}\frac{\pi}{2}\right) \right\} \Psi_i(k_u\rho) = \\ \sum\nolimits_i S_l(v_{li}) \sin\!\left(v_{li}\frac{\pi}{2}\right) \Psi_i\, (k_l\rho), \end{gathered} \tag{16}$$

$$\sum\nolimits_i v_{ui} S_u(v_{ui}) \cos \nu_{ui} \frac{\pi}{2}\, \Psi_i(k_u\rho) = n \sum\nolimits_i v_{li}\, S_l(v_{li}) \cos \nu_{li} \frac{\pi}{2}\, \Psi_i\, (k_l\rho), \tag{17}$$

where $n = {\epsilon_l}/{\epsilon_u}$ is a parameter that quantifies the electric field changes across the interface between the upper and lower media. Notably, $\Psi_i(k_u\rho)$ and $\Psi_i\ (k_l\rho)$ are different complete sets, where ν_{ui} and ν_{li} are different poles for k_u and k_l respectively. The impedance boundary condition on the surface of the cylinder is

$$E_\varphi = -Z_c H_z. \tag{18}$$

Here, it is worth mentioning that one advantage of the approach proposed in this paper compared to numerical approaches [28,29] is that the impedance boundary condition is built into the eigenfunctions of the complete sets $\Psi_i(k_u\rho)$ and $\Psi_i\ (k_l\rho)$. This leads to a more accurate representation of the solution components, which in turn enhances the physical interpretability of the modal structure [30]. Another advantage of the proposed approach is the orthogonality relation of the ρ eigenfunctions, namely,

$$\rho'\delta(\rho-\rho') = \sum_i \Psi_i\ (k\rho')\Psi_i\ (k\rho). \tag{19}$$

Utilizing this orthogonality relation within the proposed approach leads to the ability to deduce the following formulations:

$$\frac{\sin \nu_{ug}\left(\frac{\pi}{2}-\varphi'\right)}{2\nu_{ug}\cos \nu_{ug}\frac{\pi}{2}}\ \Psi_g\left(k_u\rho'\right) - S_u\left(\nu_{ug}\right)\sin\left(\nu_{ug}\frac{\pi}{2}\right) = \sum\nolimits_i S_l\left(\nu_{2i}\right)\sin\left(\nu_{li}\frac{\pi}{2}\right)\ C_{pg}\ \forall_g, \tag{20}$$

$$\nu_{ug}\ S_u\left(\nu_{ug}\right)\ cos\left(\nu_{ug}\frac{\pi}{2}\right) = n\sum_i \nu_{li}\ S_l(\nu_{li})cos\left(\nu_{li}\frac{\pi}{2}\right)\ C_{pg}\ \forall_g\ \ , \tag{21}$$

$$\text{where } C_{pg} = \int_r^\infty \frac{1}{\rho}\ \Psi_g(k_u\rho)\Psi_i(k_l\rho)\ d\rho/\rho\ , \tag{22}$$

Another advantage of the usage of the orthogonality relation of the complete sets within the proposed approach is that this provides the ability to recast the problem into a linear system on the expansion coefficients $S_u(\nu_{ui})$ and $S_l(\nu_{li})$, where the solution of this system fully defines the fields of the problem. This linear system can be formulated as

$$M - Q\left[\sin \upsilon_u\frac{\pi}{2}\right]S_u = C\ Q\ \left[\sin \upsilon_l\frac{\pi}{2}\right]\ S_l\ , \tag{23}$$

$$Q\left[\upsilon_u\cos \upsilon_u\frac{\pi}{2}\right]\ S_u = C\ Q\ \left[n\nu_l\cos \nu_l\frac{\pi}{2}\right]\ S_l\ , \tag{24}$$

where M is a vector originated from the illumination source with the elements

$$M = \left\{ \frac{\sin\left(\upsilon_{ug}(\pi/2-\varphi')\right)}{2\upsilon_{ug}\ \cos\left(\upsilon_{ug}\pi/2\right)}\ \Psi_g\left(k_u\rho'\right)\ \right\}, \tag{25}$$

And $Q[b_x]$ represents diagonal matrices with diagonal elements b_x representing the roots of the upper and lower media, C is a matrix with elements C_{pg}, and S_u and S_l are the expansion coefficient vectors of the upper and lower media respectively. The solution of the above system can be written as

$$S_u = Y^{-1}M, \tag{26}$$

$$S_l = Q^{-1}\left[n\ \nu_l\ \cos \upsilon_l\frac{\pi}{2}\right]C^{-1}\ Q\left[\nu_u\ \cos \upsilon_u\frac{\pi}{2}\right]S_u\ , \tag{27}$$

$$\text{where } Y = Q\left[\sin \upsilon_u\frac{\pi}{2}\right] + CQ\left[\sin \upsilon_l\frac{\pi}{2}\right]Q^{-1}\left[n\upsilon_l\cos \upsilon_l\frac{\pi}{2}\right]C^{-1}Q\left[\upsilon_u\cos \upsilon_u\frac{\pi}{2}\right]\ . \tag{28}$$

The solution of the derived linear system is the unknown expansion coefficients. Once the expansion coefficients of the index transform are identified, all the field components will be attained. Here, the fields' expressions are valid everywhere. Also, it is worth mentioning that any values for the cylinder radius and/or any frequency range can be used within the modal approach. For example, the developed approach can be applied, among other applications, to embedded nanowires or nanorods in photonic devices and optical antennas, as well as cylindrical elements used in filters, reflectors, and modulators.

In Figure 2, the proposed solver results were compared with frequency-domain finite element analysis solver results for 10 wavenumbers. The diamonds and circles in the figure represent the field computations of the proposed solver and the finite element solver, respectively. As shown in Figure 2, the proposed solver results are very close to those of the finite element analysis solver.

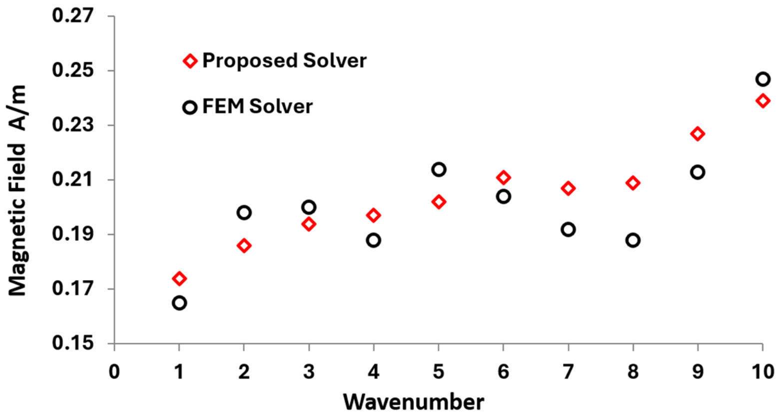

Figure 2. The proposed solver versus the finite element solver.

Also, it should be noted that the orthogonality relation for the Hankel functions of integer order in the deduced formulations represents another advantage of the proposed approach compared to other numerical approaches [31–33], where the lack of this orthogonality relation results in the appearance of additional dense matrices in the system of the form

$$\int_{r}^{\infty} H_g^{(1)}(k_u\rho)H_i^{(1)}(k_u\rho)d\rho/\rho\ , \tag{29}$$

$$\int_{r}^{\rho'} H_g^{(1)}(k_u\rho)J_i(k_u\rho)\frac{d\rho}{\rho}, \tag{30}$$

$$\int\limits_{\rho'}^{\infty} H_g^{(1)}(k_u\rho)H_i^{(1)}(k_u\rho)d\rho/\rho. \tag{31}$$

Notably, the generated matrices represented by Equations (29)–(31) are not diagonal [34]; thus, it will be a challenging task to derive a linear system formation like the one proposed in Equations (23) and (24), and this, in turn, will complicate the possibility of developing a solution approach for such cylindrical configurations.

Another edge of the proposed approach over other approaches [26,35] is related to convergence behaviour. Notably, for the approach proposed in this work, the asymptotic expansion of the used Bessel and Hankel functions as $g \to \infty$ reveals that the series representations in Equations (1)–(3) tend to converge exponentially with the order of the ith term, with $O\left(e^{j\nu_i|\varphi-\varphi'|}\right)$ for Equation (1) and $O\left(e^{j\nu_i|\varphi|+\varphi'}\right)$ for Equations (2) and (3). This leads to a faster series convergence compared to other methodologies that depend on Fourier series expansions on the angular variable, where the series convergence for such approaches may be algebraic [24,36]. Also, while the conventional finite element-based approaches require the solution of large sparse systems [37] and the finite difference time-domain methods incur a high cost due to the time stepping [38], the proven exponential convergence of the proposed approach ensures that the required number of modes for a certain level of accuracy is significantly small, hence reducing the computational cost of the matrix inversion, which is the dominant element of the computational burden [39,40].

Now, to analyze the convergence performance of the proposed approach, five configurations were selected to represent different ranges of permittivity commonly exhibited by antenna, photonics, and optics applications [41–45]. The five configurations were designed to represent different percentages of relative permittivity contrast between upper and lower media, as depicted in Table 1.

Table 1. Relative permittivity values of the five configurations studied.

Configuration Number	Relative Permittivity of the Upper Medium	Relative Permittivity of the Lower Medium	Relative Permittivity Contrast (%)
1	75	71.25	5%
2	60	45	25%
3	9	13.5	50%
4	90	22.5	75%
5	1.1	2.2	100%

To evaluate the convergence results, a relative percentage error parameter, β, was defined as follows:

$$\beta = \frac{H_{PS} - H_{FEM}}{H_{FEM}} \times 100, \tag{32}$$

where H_{PS} is the magnetic field computed using the proposed solver and H_{FEM} is the magnetic field computed using the finite element solver. The results in Figure 3 reveal that, for all the investigated configurations, as the number of modes increases, β values decrease considerably. Moreover, it can be observed that as the percentage of permittivity contrast between upper and lower media varies from 5% to 100%, more modes are needed to reach a quite small β value (0.1%). At the same time, it is shown that the adequate representation of the fields is achieved using relatively few modes for the proposed solver.

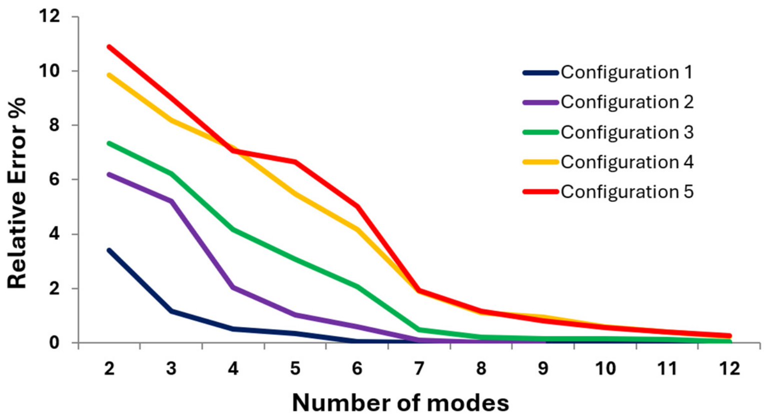

Figure 3. Relative error versus number of modes for the five studied configurations.

That said, it is worth mentioning that the elements that structure the proposed modal solver contribute to the significant avoidance of any possible ill-conditioning or numerical stability issues. First, the semi-analytical nature of the solution makes the proposed approach structured from the beginning to avoid some of the usual mechanisms that generate ill-conditioning in fully numerical methods (i.e., discretization of the modelling domain, mesh density, etc.) [46]. Second, the orthonormal structure of the complete sets used further supports stability, as each mode represents an independent physical direction in function space, which makes the proposed method physically adapted to the problem and less prone to numerical sensitivity [47]. Also, since the impedance boundary condition is built into the eigenfunctions of the complete sets, the resulting system significantly avoids a primary source of ill-conditioning encountered in discretization-based methods from approximate boundary enforcement [48].

Moreover, the use of orthogonal eigenfunctions ensures that the resulting matrix system is diagonally structured, thereby suppressing any possible coupling between coefficients and significantly improving numerical stability [49]. Furthermore, although the conditioning of the resulting linear system is not directly implied by the orthogonality of the complete sets, the exponential convergence of the proposed approach ensures that a small number of modes is required, thereby avoiding the occurrence of extreme coefficient values, which in turn greatly mitigates any potential ill-conditioning environments [50].

3. Impedance-Dominant Regime

Here, attention will be turned to a special case of this study, which is the impedance-dominant scenario [51]. In the impedance-dominant scenario, the wavenumbers of the upper and lower media are the same, "i.e., $k_u = k_l$", despite the fact that they have dissimilar impedances [52,53]. Analysis of the impedance-dominant model is mostly problematic and challenging to resolve using numerically based approaches [37,38]. On the other hand, the focus on the impedance-dominant regime is interesting, as this concept supports applications that require preservation of phase velocity continuity or dispersion, while scattering or directionality can be governed by impedance contrast only [54,55]. Therefore, the impedance-dominant regime is an important design paradigm that is relevant to designing many engineered electromagnetic systems, such as optical coatings and impedance-tailored photonic devices [56–58]. In these devices, the phase velocity is deliberately matched to preserve wavefront continuity, while the impedance can be manipulated to achieve the intended device function [59,60].

For the characterization of this regime, the proposed procedure formulations will be updated so that the values of ν_{ui} will equal the values of ν_{li}. Also, for this regime, the theoretical framework will be updated so that one orthogonal complete set is applied for both upper and lower media. Consequently, Equations (16) and (17) will be updated, where the C_{pg} quantity in Equations (20) and (21) will be made diagonal, which will lead to less dense matrices. Eventually, an updated linear system will be formulated with the following form:

$$\frac{\sin\left(v_{ug}\ (\pi/2-\varphi')\right)}{2\ v_{ug}\ \cos v_{ug}\pi/2}\ \Psi_g\left(k_u\rho'\right) - S_u\left(v_{ug}\right)\sin\left(v_{ug}\frac{\pi}{2}\right) = S_l\left(v_{ug}\right)\sin\left(v_{ug}\frac{\pi}{2}\right), \tag{33}$$

$$S_u\left(v_{ug}\right) = n\ S_l\left(v_{ug}\right). \tag{34}$$

This in turn will result in a closed-form analytic expression for both expansion coefficients, $S_u\left(v_{ug}\right)$ and $S_l\left(v_{ug}\right)$, with

$$S_l\left(v_{ug}\right) = {}^{1}\!/_{1+n}\ \frac{\sin\left(v_{ug}(\pi/2-\varphi')\right)}{2v_{ug}\ \cos v_{ug}\pi/2\ \sin\left(v_{ug}\pi/2\right)}\Psi_g\left(k_u\rho'\right). \tag{35}$$

Thus, the magnetic field representations for the upper and lower media will be reformulated as

$$H_z^l = \frac{1}{1+n}\sum\nolimits_g \frac{\sin\left(v_{ug}(\pi/2-\varphi')\right)}{2v_{ug}\cos\left(v_{ug}\pi/2\right)\ \sin\left(v_{ug}\pi/2\right)}\sin\left(v_{ug}(\varphi+\pi/2)\right)\Psi_g\left(k_u\rho'\right)\ \Psi_g\left(k_u\rho\right), \tag{36}$$

$$H_z^{u(a)} = {}^{n}\!/_{1+n}\sum\nolimits_g \frac{\sin\left(v_{ug}(\pi/2-\varphi')\right)}{2v_{ug}\cos\left(v_{ug}\pi/2\right)\ \sin\left(v_{ug}\pi/2\right)}\sin\left(v_{ug}(\varphi-\pi/2)\right)\Psi_g\left(k_u\rho'\right)\Psi_g\left(k_u\rho\right)., \tag{37}$$

For the source discontinuity field component, $H_z^{u(d)}$, the field representation in Equation (1) is valid everywhere except for a certain coincident source–observer situation, where the observer and the source are both located exactly at the interface between the two half-spaces. In this specific situation only, the proposed series representations will diverge. As a remedy for this situation, a convergent scheme for the $H_z^{u(d)}$ field representation will be derived accordingly. The first step of the convergent scheme is done through reformulating the $\left[\frac{\sin(v_{ui}(\pi/2-\varphi_>))\cos(\nu_{ui}\varphi_<)}{2\nu_{ui}\cos(\nu_{ui}\pi/2)}\right]$ term in Equation (1) as

$$\left[\frac{\sin(v_{ui}(\pi/2-\varphi_>))\cos(\nu_{ui}\varphi_<)}{2\nu_{ui}\cos(\nu_{ui}\pi/2)}\right]=\left[\frac{1}{4}\left\{je^{j\nu_{ui}|\varphi-\varphi'|}-\frac{2je^{j\pi v_{ui}}}{1+e^{j\pi v_{ui}}}\cos v_{ui}(\varphi-\varphi')+\frac{\sin(v_{ui}(\pi/2-\varphi-\varphi'))}{\cos\nu_{ui}\pi/2}\right\}\right] \tag{38}$$

By substituting this representation into the $H_z^{u(d)}$ field expression in Equation (1) in the special situation along $\varphi=\varphi'$, the second and the third parts of this new representation will result in a convergent series for all observation angles. However, the first part of the new representation still needs to be handled for efficient computation of the field expression. The first part of the new representation is dealt with here using the Watson transform [61]. The Watson transform is a well-established technique that is used to convert a series over integer indices into an integral over a complex contour [62–64]. The technique demonstrates its applicability as a working tool in developing solutions for several applications, from scattering and diffraction problems to quantum and condensed matter systems [65–68]. It is worth mentioning that other rigorous techniques such as the Abel–Plana formula [69] and the Mellin–Barnes transform [70] were developed to convert a discrete series over integers or modes into a complex integral representation. While Abel–Plana is often simpler and Mellin–Barnes is a more general technique, both are relatively less well suited to wave problems [71,72]. On the other hand, the Watson transform is applicable in wave scattering applications as it preserves the physical interpretation of the wave problem [73,74].

Once the Watson transform is applied to the first part of the new representation in Equation (38), the following expression can be derived:

$$\frac{i}{16}\left[\int_\delta e^{j\nu|\varphi-\varphi'|}\left\{H_\nu^{(2)}(k_u\rho_<)H_\nu^{(1)}(k_u\rho_>)-H_\nu^{(1)}(k_u\rho)H_\nu^{(1)}(k_u\rho')\frac{H_\nu^{(2)}(k_ur)}{H_\nu^{(1)}(k_ur)}\right\}d\nu\right], \tag{39}$$

where δ is the contour around the zeros of $d(\nu)=0$ in the first quadrant of the complex ν plane and $H_\nu^{(1)}(.)$ and $H_\nu^{(2)}(.)$ are the Hankel functions of the first/second kind and complex order, ν. The resultant transformation is designed to improve the mathematical handling of the field expression, and it makes it more amenable to asymptotic evaluation [75,76]. Hence, the asymptotic evaluation of Equation (39) leads to the conclusion that the derived integrals can be recognized as the geometrical optical incident and reflected fields respectively [77,78]. Thus, the proposed remedy approach is now complete, and one can plug the formulation defined by Equation (38) into Equation (1) to get a convergent representation of the $H_z^{u(d)}$ field in the special situation along $\varphi=\varphi'$.

4. Conclusions

In this paper, the modelling of the interaction of electromagnetic fields with a cylindrical object situated between piecewise homogeneous media comprising two homogeneous half-spaces with asymmetric electromagnetic properties is addressed. A procedure is proposed to solve this problem that involves the formulation of the electromagnetic fields in terms of a complete orthonormal set that depends on expansion coefficients of the Hankel function transform. The proposed procedure takes advantage of the orthogonality feature of the Hankel functions of integer order to attain a linear system that comprises the unidentified expansion coefficients to deduce the electromagnetic fields of the model.

The presented procedure possesses the advantages of incorporating the impedance boundary condition directly into the eigenfunctions of the proposed complete set, which leads to more accurate modal representations. Furthermore, the proposed procedure holds the advantage of an exponential convergence for the series representations of the fields' components.

On the other hand, the proposed procedure delves into the impedance-dominant regime, where the field's representations are updated accordingly. Additionally, within this regime, the special case of a coincident source–observer situation at the interface between the two half-spaces was treated using the Watson transform technique, where a convergent scheme was deduced for the solution, which is to be understood in its asymptotic sense.

It will be of interest to investigate the development of the presented approach in the case of rough-surface cylindrical configurations. This should be investigated in future work. Also, it is worth mentioning that the formulations of the proposed procedure generalize the theoretical framework so that it can deal with electromagnetic fields in the presence of other sources of excitation, such as plane waves or beams, for the same geometry as the one presented here. Furthermore, the presented procedure may also be extended for the solution of electromagnetic scattering problems associated with other geometries, such as a cylinder in the vicinity of two half-spaces and a cylinder less/more than half buried, which will be studied in future work. Finally, the proposed procedure can be further developed to address the forward model based on the transverse magnetic (TM) approach, which will also be investigated in future work.

Funding: This research received no external funding.

Data Availability Statement: The data are contained within the article.

Acknowledgments: The author is grateful to Aladin Kamel, Advanced Industrial, Technical and Engineering Center, for his fruitful guidance during the development of this work.

Conflicts of Interest: The author declares no conflicts of interest.

References

1. Ishimaru, A. *Electromagnetic Wave Propagation, Radiation, and Scattering: From Fundamentals to Applications*, 2nd ed.; John Wiley & Sons: Hoboken, NJ, USA, 2017. [CrossRef]
2. Ida, N. *Engineering Electromagnetics*, 4th ed.; Springer: New York, NY, USA, 2020. [CrossRef]
3. LoVetri, J.; Asefi, M.; Gilmore, C.; Jeffrey, I. Innovations in electromagnetic imaging technology. *IEEE Antennas Propag. Mag.* **2020**, *62*, 33–42. [CrossRef]
4. Khan, A.S.; Mukerji, S.K. *Electromagnetic Fields: Theory and Applications*, 1st ed.; CRC Press: Boca Raton, FL, USA, 2020. [CrossRef]
5. Gbur, G.J. *Electromagnetic Optics*, 1st ed.; IOP Publishing: London, UK, 2025. [CrossRef]
6. Bickers, N.E. *Classical Optics and Electromagnetic Waves*, 1st ed.; CRC Press: Boca Raton, FL, USA, 2026.
7. Elkattan, M. An efficient technique for solving inhomogeneous electromagnetic inverse scattering problems. *J. Electromagn. Eng. Sci.* **2020**, *20*, 64–72. [CrossRef]
8. Ullah, H.; Awan, Z.A. Scattering of electromagnetic waves from a thin triangular dielectric disk. *Optik* **2021**, *227*, 165224. [CrossRef]
9. Ahmad, Z.; Awan, Z.A.; Hussain, A. Electromagnetic characteristics of a metasurface composed of uncoated and coated spherical particles. *Optik* **2020**, *220*, 165103. [CrossRef]
10. Elkattan, M. Reconstruction of induced polarization information from electromagnetic data using neural network approach. *J. Electromagn. Eng. Sci.* **2025**, *25*, 307–317. [CrossRef]
11. Morán-López, A.; Córcoles, J.; Ruiz-Cruz, J.A.; Montejo-Garai, J.R.; Rebollar, J.M. Electromagnetic scattering at the waveguide step between equilateral triangular waveguides. *Adv. Math. Phys.* **2016**, *1*, 2974675. [CrossRef]
12. Tabatadze, V.; Alperen, Ö.F.; Karaçuha, K. Electromagnetic scattering of H-polarised cylindrical wave by a double-sided impedance circular strip. *IET Microw. Antennas Propag.* **2023**, *17*, 1093–1105. [CrossRef]
13. Inan, U.S.; Marshall, R.A. *Numerical Electromagnetics: The FDTD Method*, 1st ed.; Cambridge University Press: Cambridge, UK, 2011.
14. Cardoso, J.R.; Coelho, R.R.A. *Electromagnetics Through the Finite Element Method: A Simplified Approach Using Maxwell's Equations*, 2nd ed.; CRC Press: Boca Raton, FL, USA, 2025. [CrossRef]
15. Kamel, A.H. Cost-effective schemes for the numerical simulation of electromagnetic waves. *J. Electromagn. Waves Appl.* **1994**, *8*, 693–710. [CrossRef]

16. Kamel, A.; Sguazzero, P.; Kindelan, M. Cost-effective staggered schemes for the numerical simulation of wave propagation. *Int. J. Numer. Methods Eng.* **1995**, *38*, 755–773. [CrossRef]
17. Kamel, A.H. On the accuracy of absorbing boundary conditions for wave propagation. *J. Electromagn. Waves Appl.* **1994**, *8*, 647–657. [CrossRef]
18. Elkattan, M.; Kamel, A. Characterization of electromagnetic parameters through inversion using metaheuristic technique. *Inverse Probl. Sci. Eng.* **2021**, *29*, 567–585. [CrossRef]
19. Elkattan, M.; Kamel, A.H. A novel representation of electromagnetic field interaction with vertically stratified structures. *COMPEL* **2023**, *42*, 1624–1640. [CrossRef]
20. Rao, T.C.; Barakat, R. Plane-wave scattering by a conducting cylinder partially buried in a ground plane. 1. TM case. *J. Opt. Soc. Am. A* **1989**, *6*, 1270–1280. [CrossRef]
21. Rao, T.C.; Barakat, R. Plane-wave scattering by a conducting cylinder partially buried in a ground plane II: TE case. *J. Opt. Soc. Am. A* **1991**, *8*, 1986–1990. [CrossRef]
22. Saiz, J.M.; Valle, P.J.; González, F.; Ortiz, E.M.; Moreno, F. Scattering by a metallic cylinder on a substrate: Burying effect. *Opt. Lett.* **1996**, *21*, 1330–1332. [CrossRef]
23. Di Vico, M.; Frezza, F.; Pajewski, L.; Schettini, G. Scattering by buried dielectric cylindrical structures. *Radio Sci.* **2005**, *40*, 1–11. [CrossRef]
24. Pajewski, L.; Schettini, G.; Frezza, F. Cylindrical-wave approach for the electromagnetic scattering problem by buried two-dimensional objects. *J. Appl. Geophys.* **2009**, *67*, 318–326. [CrossRef]
25. Frezza, F.; Pajewski, L.; Ponti, C.; Schettini, G.; Tedeschi, N. Electromagnetic scattering by a metallic cylinder buried in a lossy medium with the cylindrical-wave approach. *IEEE Geosci. Remote Sens. Lett.* **2012**, *10*, 179–183. [CrossRef]
26. Hamid, A.K.; Cooray, F. Scattering from a buried PEMC cylinder due to a line source excitation above a planar interface between two isorefractive half spaces. *Adv. Electromagn.* **2019**, *8*, 1–6. [CrossRef]
27. Osipov, A.V.; Tretyakov, S.A. *Modern Electromagnetic Scattering Theory with Applications*, 1st ed.; John Wiley & Sons: Chichester, UK, 2017. [CrossRef]
28. Ozzaim, C. A simple numerical solution method for TM scattering by conducting cylinders partially buried in a dielectric half-space. *Prog. Electromagn. Res. Lett.* **2020**, *88*, 51–57. [CrossRef]
29. Ozzaim, C. A MoM solution for TM scattering by dielectric cylinders above an infinite flat surface. *J. Mod. Opt.* **2019**, *66*, 1550–1557. [CrossRef]
30. Felsen, L.B.; Marcuvitz, N. *Radiation and Scattering of Waves*; IEEE Press: New York, NY, USA, 1994. [CrossRef]
31. Kouroublakis, M.; Tsitsas, N.L.; Leviatan, Y. A time-domain method of auxiliary sources for efficient analysis of transient electromagnetic scattering by moderately conductive cylinders. *Eng. Anal. Bound. Elem.* **2026**, *183*, 106605. [CrossRef]
32. Tsitsas, N.L.; Zouros, G.P.; Fikioris, G.; Leviatan, Y. On methods employing auxiliary sources for 2-D electromagnetic scattering by noncircular shapes. *IEEE Trans. Antennas Propag.* **2018**, *66*, 5443–5452. [CrossRef]
33. Cheng, A.H.; Hong, Y. An overview of the method of fundamental solutions—Solvability, uniqueness, convergence, and stability. *Eng. Anal. Bound. Elem.* **2020**, *120*, 118–152. [CrossRef]
34. Kumagai, N.; Morita, N.; Mautz, J.R. *Integral Equation Methods for Electromagnetics*; Artech House Publishers: Boston, MA, USA, 1991.
35. Shahzad, A.; Ahmed, S.; Naqvi, Q.A. Analysis of electromagnetic field due to a buried coated PEMC circular cylinder. *Opt. Commun.* **2010**, *283*, 4563–4571. [CrossRef]
36. Di Vico, M.; Frezza, F.; Pajewski, L.; Schettini, G. Scattering by a finite set of perfectly conducting cylinders buried in a dielectric half-space: A spectral-domain solution. *IEEE Trans. Antennas Propag.* **2005**, *53*, 719–727. [CrossRef]
37. Jin, J.M. *The Finite Element Method in Electromagnetics*, 3rd ed.; John Wiley & Sons: Hoboken, NJ, USA, 2014.
38. Taflove, A.; Hagness, S.C. *Computational Electrodynamics: The Finite-Difference Time-Domain Method*, 3rd ed.; Artech House: Boston, MA, USA, 2005. [CrossRef]
39. Elkattan, M.; Kamel, A.H. Estimation of electromagnetic properties for 2D inhomogeneous media using neural networks. *J. Electromagn. Eng. Sci.* **2022**, *22*, 152–161. [CrossRef]
40. Elkattan, M.; Kamel, A. Characterization of induced polarization parameters from electromagnetic data using evolutionary approach. *J. Electromagn. Eng. Sci.* **2023**, *23*, 303–309. [CrossRef]
41. O'Keefe, S.G.; Kingsley, S.P. Tunability of liquid dielectric resonator antennas. *IEEE Antennas Wirel. Propag. Lett.* **2007**, *6*, 533–536. [CrossRef]
42. Sivan, A.; Muhammed Azeem, V.; Kumar, N.; Murali, K.M.P. Design and Fabrication of a Microstrip Patch Antenna Using a Flexible Low-Dielectric, Low-Loss Substrate. *Phys. Status Solidi A* **2025**, *222*, e202500550. [CrossRef]
43. Luukkonen, O.; Costa, F.; Simovski, C.R.; Monorchio, A.; Tretyakov, S.A. A thin electromagnetic absorber for wide incidence angles and both polarizations. *IEEE Trans. Antennas Propag.* **2009**, *57*, 3119–3125. [CrossRef]
44. Wu, D.; Pak, A.J.; Liu, Y.; Zhou, Y.; Wu, X.; Zhu, Y.; Lin, M.; Han, Y.; Ren, Y.; Peng, H.; et al. Thickness-dependent dielectric constant of few-layer In2Se3 nanoflakes. *Nano Lett.* **2015**, *15*, 8136–8140. [CrossRef] [PubMed]

45. Thomas, P.; Satapathy, S.; Dwarakanath, K.; Varma, K.B.R. Dielectric properties of poly (vinylidene fluoride)/CaCu3Ti4O12 nanocrystal composite thick films. *arXiv* **2013**, arXiv:1301.4056. [CrossRef]
46. Volakis, J.L.; Sertel, K. *Integral Equation Methods for Electromagnetics*; SciTech Publishing: Raleigh, NC, USA, 2012. [CrossRef]
47. Chari, M.V.; Salon, S. *Numerical Methods in Electromagnetism*; Academic Press: San Diego, CA, USA, 2000.
48. Sheng, X.Q.; Song, W. *Essentials of Computational Electromagnetics*; John Wiley & Sons: Singapore, 2012.
49. Sadiku, M.N.O. *Numerical Techniques in Electromagnetics*, 2nd ed.; CRC Press: Boca Raton, FL, USA, 2000.
50. Jin, J.M. *Theory and Computation of Electromagnetic Fields*, 2nd ed.; John Wiley & Sons: New York, NY, USA, 2015.
51. Grahn, P.; Shevchenko, A.; Kaivola, M. Theoretical description of bifacial optical nanomaterials. *Opt. Express* **2013**, *21*, 23471–23485. [CrossRef]
52. Collin, R.E. *Foundations for Microwave Engineering*, 2nd ed.; John Wiley: Hoboken, NJ, USA, 2001. [CrossRef]
53. Stratton, J.A. *Electromagnetic Theory*; Wiley-IEEE Press: New York, NY, USA, 2007.
54. Dang, Z.; Faul, F.; Palm, D.; Fip, T.; Kappa, J.; Becker, S.; Rahm, M. Impedance-matched planar metamaterial beam steerer for terahertz waves. *arXiv* **2020**, arXiv:2005.09274. [CrossRef]
55. Asadchy, V.S.; Albooyeh, M.; Tcvetkova, S.N.; Díaz-Rubio, A.; Ra'di, Y.; Tretyakov, S.A. Perfect control of reflection and refraction using spatially dispersive metasurfaces. *Phys. Rev. B* **2016**, *94*, 075142. [CrossRef]
56. Lawrence, F.J.; de Sterke, C.M.; Botten, L.C.; McPhedran, R.C.; Dossou, K.B. Modeling photonic crystal interfaces and stacks: Impedance-based approaches. *Adv. Opt. Photon.* **2013**, *5*, 385–455. [CrossRef]
57. Li, Y.; Sun, X.; Shen, H.; Hu, X. Impedance-matched metadevices with a single matrix material. *Sci. Rep.* **2025**, *15*, 17264. [CrossRef]
58. Kim, K.H.; Park, Q.H. Perfect anti-reflection from first principles. *Sci. Rep.* **2013**, *3*, 1062. [CrossRef]
59. Wu, M.; He, X.; Lu, G.; Zhang, Y.; Geng, Z.; Liu, H.; Zhang, K. On-chip multi-channel wavefront manipulation of spoof surface waves with structural heterogeneous metasurfaces. *Laser Photonics Rev.* **2026**, *20*, e01634. [CrossRef]
60. Chen, X.D.; Wang, E.H.; Shan, L.K.; Feng, C.; Zheng, Y.; Dong, Y.; Guo, G.C.; Sun, F.W. Focusing the electromagnetic field to 10^{-6} λ for ultra-high enhancement of field-matter interaction. *Nat. Commun.* **2021**, *12*, 6389. [CrossRef]
61. Valagiannopoulos, C. An overview of the watson transformation presented through a simple example. *Prog. Electromagn. Res.* **2007**, *75*, 137–152. [CrossRef]
62. Hussar, P.E.; Smith-Rowland, E.M. An asymptotic solution for boundary layer fields near a convex impedance surface. *J. Electromagn. Waves Appl.* **2002**, *16*, 185–208. [CrossRef]
63. Shim, J.; Kim, H.T. Dominance of creeping wave modes of backscattered field from a conducting sphere with dielectric coating. *Prog. Electromagn. Res.* **1999**, *21*, 293–306. [CrossRef]
64. Andropov, I.V.; Bouche, D. Asymptotics of creeping waves in a degenerated case of matrix impedance. *Prog. Electromagn. Res.* **2006**, *59*, 215–230. [CrossRef]
65. Kim, H.T. High-frequency analysis of EM scattering from a conducting sphere coated with a composite-material. *IEEE Trans. Antennas Propag.* **1993**, *41*, 1665–1674. [CrossRef]
66. Shim, J.; Kim, H.T. An asymptotic solution of EM backscattering from a conducting sphere coated with a composite material. *IEEE Trans. Antennas Propag.* **2004**, *52*, 1465–1472. [CrossRef]
67. Valagiannopoulos, C.; Kovanis, V. Watson transform in quantum scattering. *Sci. Rep.* **2025**, *15*, 37182. [CrossRef]
68. Sha, W.E.; Chew, W.C. High frequency scattering by an impenetrable sphere. *Prog. Electromagn. Res.* **2009**, *97*, 291–325. [CrossRef]
69. Saharian, A.A. The generalized Abel-Plana formula with applications to Bessel functions and Casimir effect. *arXiv* **2007**, arXiv:0708.1187. [CrossRef]
70. Allendes, P.; Guerrero, N.; Kondrashuk, I.; Notte Cuello, E.A. New four-dimensional integrals by Mellin–Barnes transform. *J. Math. Phys.* **2010**, *51*, 052304. [CrossRef]
71. Campos, R.G.; Díaz, F.M. Quadrature formulas for the Laplace and Mellin transforms. *BIT Numer. Math.* **2009**, *49*, 477–486. [CrossRef]
72. Luchko, Y.; Kiryakova, V. The Mellin integral transform in fractional calculus. *Fract. Calc. Appl. Anal.* **2013**, *16*, 405–430. [CrossRef]
73. Li, M.K.; Chew, W.C. A new Sommerfeld-Watson transformation in 3-D. *IEEE Antennas Wirel. Propag. Lett.* **2004**, *3*, 75–78. [CrossRef]
74. Wang, H.L.; Wu, Q.; He, X.J.; Li, L.W. Computation of wave scattering problems from a spheric body: Derivation of the new Sommerfeld-Watson transformation. In Proceedings of the Progress in Electromagnetics Research Symposium, Hangzhou, China, 22–26 August 2005; Volume 707, pp. 22–26.
75. Whittaker, E.T.; Watson, G.N. *A Course of Modern Analysis*, 4th ed.; Cambridge University Press: Cambridge, UK, 1996. [CrossRef]
76. Balanis, C.A. *Advanced Engineering Electromagnetics*, 3rd ed.; John Wiley & Sons: Hoboken, NJ, USA, 2024.

77. Kravtsov, Y.A.; Orlov, Y.I. *Caustics, Catastrophes and Wave Fields*, 1st ed.; Springer: Berlin/Heidelberg, Germany, 1993. [CrossRef]
78. Solimeno, S. *Guiding, Diffraction, and Confinement of Optical Radiation*, 1st ed.; Academic Press: Cambridge, MA, USA, 1986. [CrossRef]